Desalination and Water Treatment
www.deswater.com

doi: 10.1080/19443994.2015.1100553

57 (2016) 19374–19390
September

Taylor & Francis
Taylor & Francis Group

Magnetically modified multiwalled carbon nanotubes for the adsorption of bismarck brown R and Cd(II) from aqueous solution: batch and column studies

Tabrez A. Khan*, Momina Nazir, Equbal A. Khan

Department of Chemistry, Jamia Millia Islamia, New Delhi 110 025, India, Tel. +91 11 26985938; Fax: +91 11 26985507; email: takhan501@yahoo.com (T.A. Khan), Tel. +91 9596052525; email: mominanazir1987@gmail.com (M. Nazir), Tel. +91 9953935498; email: eakhan.chem@gmail.com (E.A. Khan)

Received 28 August 2014; Accepted 20 September 2015

ABSTRACT

In this study, ferrofluid-modified multiwalled carbon nanotubes (MMWCNT) was used as an efficient adsorbent for the removal of bismarck brown R (BBR) and Cd(II) ions from aqueous solution using batch and column operations. An adsorption capacity (q_m) of 76.92 and 38.17 mg/g was achieved for BBR and Cd(II), respectively. A maximum column adsorption capacity was 98.16 and 39.15 mg/g for BBR and Cd(II), respectively. The column experimental data conformed to Thomas model. The experimental data were best fitted into Langmuir isotherm suggesting homogenous, monolayer adsorption of both the dye and metal on MMWCNT surface. The energy obtained from DKR isotherm for BBR (2.24 kJ/mol) and Cd(II) (1.58–7.07 kJ/mol) indicated physical adsorption. The adsorption of both dye and metal followed pseudo-second-order kinetics and the mechanism was both liquid film and intraparticle diffusion controlled. The adsorption process was thermodynamically spontaneous and endothermic in nature.

Keywords: Adsorption; Modified MWCNT; Bismarck brown R; Cd(II); Isotherms; Kinetics; Column studies

1. Introduction

The discharge of many hazardous dyes and/or heavy metals containing effluents from various industries into nearby water bodies are major environmental concerns due to their detrimental effects on aquatic life. Bismarck brown R (BBR) is a cationic diazo dye used mainly in colouring paper, wool and leather. Its ingestion may cause respiratory problems, skin damage and irritation [1] and is also reported to have carcinogenic effects [2]. Cadmium poisoning may also cause acute nervous damage, renal damage and hypertension. Therefore, the removal of hazardous dyes and/or metals from wastewater before they finally enter into the water bodies has gained much attention. Adsorption technology is an efficient and economically viable process for the removal of dyes and heavy metals from wastewater [3–6] owing largely to its ease of operation, simplicity of design and insensitivity to toxic pollutants [7]. Recently, there has been an increased focus on the utilization of carbon nanotubes as adsorbents for wastewater purification [8–14] mainly due its high chemical stability, hollow and layered structure, and large specific surface area.

*Corresponding author.

Since its discovery in 1991 the carbon nanotubes (CNTs), sheet(s) of graphite wrapped into a tubular structure, have received considerable attention for many applications including water treatment. CNTs are generally synthesized by arc evaporation method, laser ablation, chemical vapour deposition, electrolysis and flame synthesis, but arc evaporation, laser ablation, and chemical vapour deposition are most commonly used methods. The CNTs generally exist in single-walled CNTs (SWCNTS) or multi-walled CNTs (MWCNTS) conformations. SWCNTs consist of a single layer graphite sheet, while MWCNTs have two or more cylindrical graphitic sheets. The adsorption of pollutants onto CNTs can occur onto four sites (a) hollow interior of individual nanotubes—internal sites, (b) the interstitial channels between individual nanotubes in the bundles—interstitial channels, (c) the grooves on the periphery of a nanotube bundle and the outer surface of the outermost nanotubes, where two adjacent parallel tubes meet—grooves and (d) the curved surface of individual nanotubes on the outside of the nanotube bundles—outside surface [15]. The adsorptive surface of the raw CNTs can readily be modified by physicochemical treatments, which enhances the dispersion property and adsorption capacity. The treatment of pristine CNTs with strong oxidizing agents introduces various functional groups (COOH, OH) on its surface, which increase the affinity of CNTs towards various pollutants. However, the application of CNTs in wastewater treatment is limited due to difficulties associated with its separation. In order to overcome the disadvantage of separation difficulty, magnetic separation of magnetically modified CNTs is considered a desirable technique. Although magnetic composite/nanocomposites have been widely used in adsorption studies [16], the application of magnetic CNTs for adsorptive removal of organic dyes and metal ions from aqueous solution [17–22] is limited. Moreover, the adsorptive removal of organic dyes and metals by magnetically modified MWCNTs using batch and fixed-bed method is relatively scarce.

In this study, the magnetically modified multiwalled carbon nanotubes (MMWNTs), prepared using aqueous ferrofluid, was used for the adsorptive removal of BBR and Cd(II) from aqueous solution using both batch and fixed-bed techniques.

2. Experimental

2.1. Reagents and chemicals

MWCNTs (95%, 20–30 nm diameter) (SES Research, TX, USA), sodium hydroxide, ferrous sulphate, ferric chloride, dithizone (Merck, India), nitric acid (Qualigens, India), cadmium nitrate tetrahydrate, hydrochloric acid (s.d. fine), cetyltrimethylammonium bromide (CTAB) (Sigma Aldrich, India), BBR (CDH, India), and sulphuric acid (Himedia, India) were used as received.

2.2. Preparation of adsorbent

MWCNTs were oxidized using HNO_3 according to reported procedure [23]. Aqueous ferrofluid was prepared according to the reported method [24]. Mixed solutions of $FeCl_2$ (2 M) and $FeCl_3$ (1 M) were magnetically stirred and to it was added 100 mL of NH_4OH (0.7 M) slowly. A black precipitate of magnetite (Fe_3O_4) nanoparticles thus obtained was centrifuged for 1 min at 1,000 rpm. The supernatant was decanted and solid magnetite was treated with aqueous tetramethylammonium hydroxide (TMAH) (25%) solution. The crystallites obtained were then washed with double-distilled water to remove any impurities and resuspended in distilled water. A known weight of 2 g of MWCNT was suspended in 30 mL ethanol, and 3 mL of the prepared ferrofluid was added and the solution stirred under nitrogen atmosphere for 30 min at room temperature (25 ± 5°C). The adsorbent was finally washed with ethanol and dried at 70°C overnight.

2.3. Preparation of adsorbate solution

The stock solutions of BBR and Cd(II) (100 mg/L) were prepared by dissolving 100 mg of BBR and 280 mg of cadmium(II) nitrate tetrahydrate in 1 L of bidistilled water. Stock solutions were then diluted to desired concentrations.

2.4. Characterization of the adsorbent

The infrared spectra (4,000–400 cm^{-1}) of samples were recorded on a Perkin Elmer FT-IR BX2 instrument. The pellets were prepared by mixing 2 mg of the powdered sample with 200 mg of spectroscopic grade KBr. Scanning Electron Microscope (JEOL, model 3300) was used to investigate the surface morphology of the adsorbent. Brunauer–Emmett–Teller (BET), Barret–Joyner–Halenda (BJH) and Dubinin–Astakhov (DA) methods were used to analyse surface area, pore volume and pore radius of the adsorbent on a Nova 2000e, Quantachrome Instruments, Florida, USA. Magnetic studies were carried out using Microsense EV9 Vibrating sample magnetometeric (VSM).

2.5. Adsorption studies

Adsorption experiments were carried out at a fixed agitation speed at room temperature (298–303 K) under batch mode technique. Hundred millilitres of adsorbate solution of desired concentration (5–25 mg/L) was equilibrated with varying doses of MMWCNT in a thermostatic water bath shaker for different time intervals. The adsorbent was separated from the solution by centrifugation (REMI, R-24) and the residual concentration of adsorbate in the supernatant was determined spectrophotometrically at 465 nm for BBR and 540 nm for Cd(II). The spectrophotometric determination of Cd(II) was done following standard procedure using dithizone as a complexing agent [25]. In a typical procedure, 5 mL of dithizone solution and 2 mL of HCl (0.1 M) was mixed with 100 mL of Cd(II) solution in a calibrated flask, and to it was added 5 mL of 0.3 M CTAB. A pink coloured Cd(II)–dithizone complex was formed, the absorbance of which was measured at λ_{540} nm along with the corresponding blank. The concentration of Cd(II) was determined using the calibration curve.

The amount of adsorbate adsorbed per unit mass of the adsorbent (q_e, mg/g) was calculated using the following equation (Eq. (1)):

$$q_e = (C_o - C_e)/m \tag{1}$$

The per cent adsorption was calculated from the relationship (Eq. (2)):

$$\% \text{ adsorption} = 100\ (C_o - C_e)/C_o \tag{2}$$

where C_o is initial dye/metal concentration in mg/L before adsorption, C_e is equilibrium concentration of dye/metal in mg/L after adsorption and m is the amount of adsorbent (g/L of adsorbate solution).

For column experiments, two columns each of diameter 1.3 cm, length 1.0 cm and 2.5 cm were packed with 1.0 and 2.5 g of the adsorbent for BBR and Cd(II), respectively. The experimental set-up is diagrammatically represented in Fig. 1. The adsorbate solutions (100 mg/L) were passed through the column at a flow rate of 20 mL/min. The retention time of adsorbate was 80 min for BBR and 90 min for Cd(II). The effluent was collected in 50 mL aliquots and analysed spectrophotometrically to determine the remaining concentration of adsorbate. The column was allowed to run till the adsorbate concentration in the effluent reached around 95% of the initial concentration. Maximum column capacity (q_c) was calculated using the following equations:

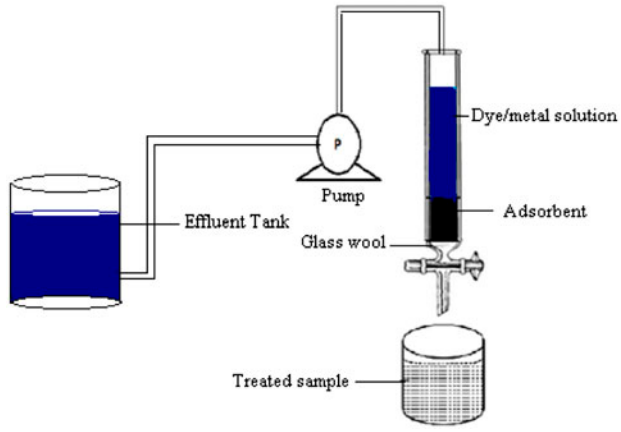

Fig. 1. Diagrammatic representation of column set-up.

$$q_{total} = A \cdot Q \cdot 1/1000 \tag{3}$$

$$q_c = q_{total}/M \tag{4}$$

where q_{total} (mg) is the total amount of dye/metal adsorbed, A is the area under C_{ad} vs. t ($C_{ad} = C_o - C_t$) curve, Q (mL/min) is the flow rate, C_o (mg/L), C_t is the concentration of the effluent after time t is the initial concentration of the influent and M is the amount of adsorbent packed in the column.

For kinetic measurements, the experiments were performed using a fixed adsorbent dose with varying contact times at different dye/metal ion concentrations. The effect of varying solution pH on adsorption was studied in the range of 2–10. The solution pH was adjusted with dilute HCl or NaOH solution (both 0.01 M). The experiments were repeated three times and average values were taken.

3. Results and discussion

3.1. Characterization of the adsorbent

3.1.1. FTIR studies

The FT-IR spectra of MMWCNT, before and after adsorption, are given in Fig. 2. The absorption peaks at 3,422 and 2,974 cm^{-1} correspond to C–H and O–H stretching, respectively. The bands due to C=O stretching modes of –COOH groups on the surface of the MMWCNTs was observed at 1,740 cm^{-1}. The band at 1,635 cm^{-1} is assigned to anti-symmetric C–O stretch, whereas the band at 1,593 cm^{-1} is attributed to C=C stretch. The R–O–R stretch and characteristic Fe–O stretching vibrations appeared in the spectrum at 1,294 and 586 cm^{-1}. After adsorption, no appreciable

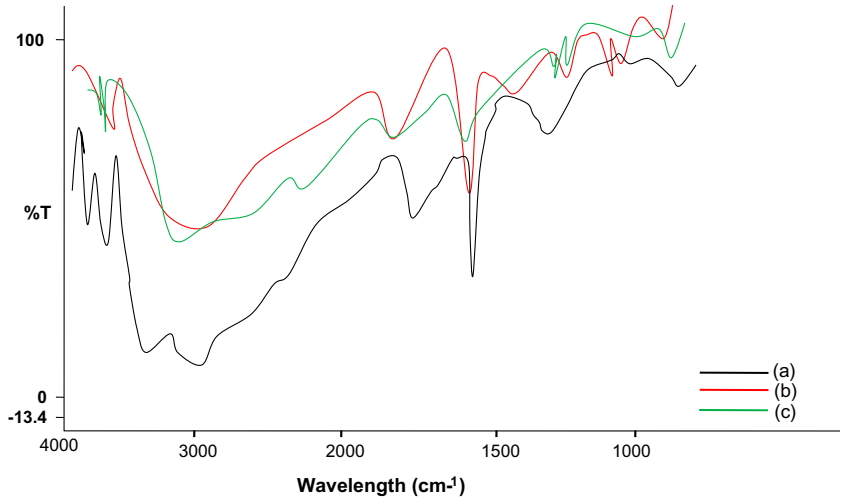

Fig. 2. FT-IR spectrum of MMWCNT (a) before adsorption, (b) after BBR adsorption and (c) after Cd(II) adsorption.

changes in the absorption bands were observed, which pointed out the physical nature of adsorbent–adsorbate interaction. New peaks at 1,046 and 1,102 cm^{-1} were attributed to C–H bending vibration of aromatic ring and C–N stretching vibration of the adsorbed BBR molecules.

3.1.2. Scanning electron microscopic studies

The SEM images of the adsorbent are given in Fig. 3(a) and (b). It is clear from the images that iron oxide nanoparticles or their aggregates are deposited on the nanotube walls. The SEM images of MMWCNT

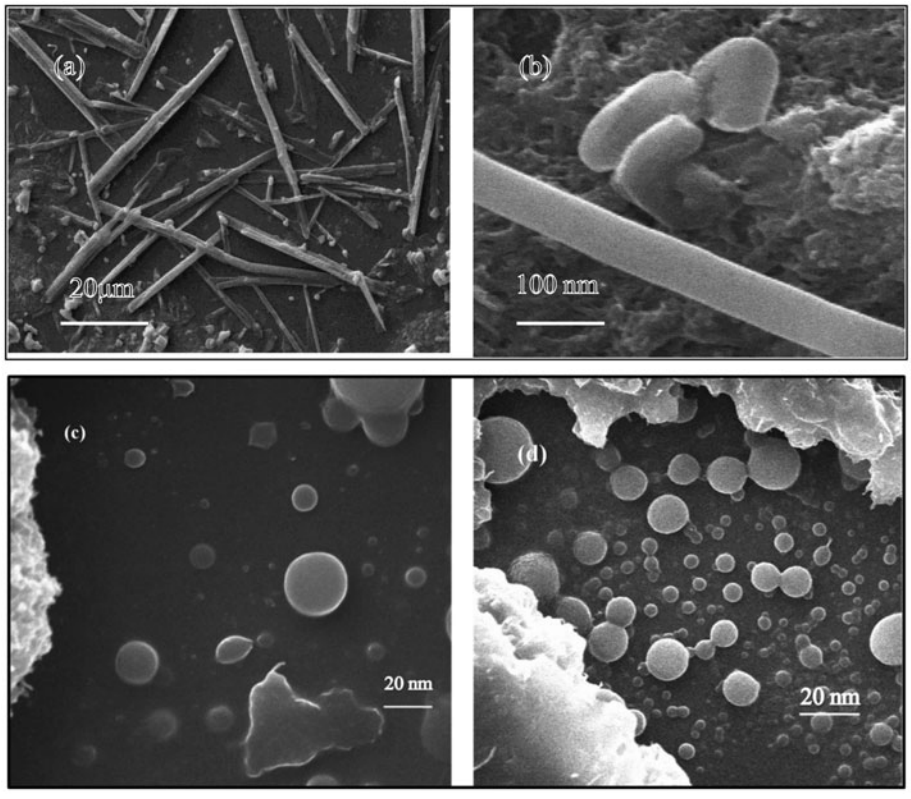

Fig. 3. SEM images of MMWCNT (a), (b) before adsorption, (c) after Cd(II) adsorption and (d) after BBR adsorption.

after adsorption (Fig. 3(c) and (d)) show the adsorbed Cd(II) ions and BBR molecules adhering onto the adsorbent surface and interior pores.

3.1.3. Surface area and porosity measurements

Based on the BET, BJH, DA method, the specific surface area, pore radius and pore volume were estimated and are given in Table 1. BET surface area was 399.67 m^2/g which was high compared to pristine MWCNTs (outer diameter 10–30 nm, length 1–100 μm) being 158–162 m^2/g [26]. Pore radius indicated mesoporous nature of the adsorbent.

3.1.4. VSM analysis

The magnetization curve (Fig. 4) showed no permanent magnetization. Neither coercivity nor remanence was observed indicating the superparamagnetic nature of the adsorbent. This property of losing magnetic nature, in absence of external magnetic field, made it possible for the adsorbent to retain its surface area and active sites while adsorption without aggregating [27]. Moreover, it shows a good saturation magnetization of ~19.16 emu/g which is greater than reported earlier (4.81 emu/g) [28].

Table 1
Surface area properties of MMWCNT

Method	Surface area (m^2/g)	Pore radius (nm)	Pore volume (cm^3/g)
BET	399.67	–	–
BJH	241.74	1.60	1.09
DA	–	1.17	0.82

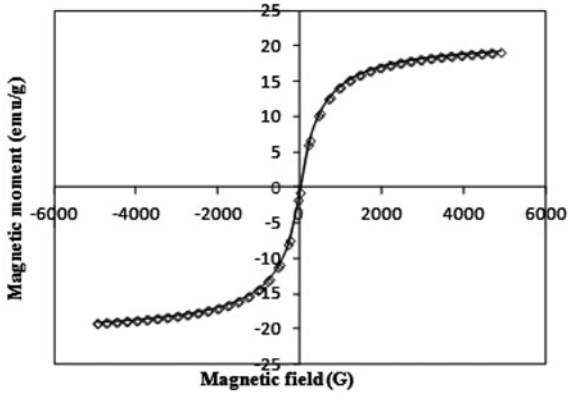

Fig. 4. Magnetization curve of MMWCNT.

3.2. Equilibrium adsorption studies

3.2.1. Effect of contact time

The effect of contact time on the adsorption of BBR and Cd(II) onto MMWCNT was studied at a constant adsorbent dose of 0.1 and 0.5 g/L for BBR and Cd(II), respectively, and is depicted in Fig. 5(a) and (b).With increase in contact time from 10 to 100 min, q_e increased from 98.17 (49.08%) to 176.42 mg/g (88.21%) for BBR attaining equilibrium at 80 min. For Cd(II) removal, with an increase in contact time from 5 to 30 min, q_e increased from 22.61 (90.43%) to 23.93 mg/g (95.71%) reaching equilibrium at 20 min. This trend can be explained as: initially the surface of the adsorbent had sufficient vacant sites and the longer contact between adsorbent and adsorbate increased the access of these vacant sites to the dye and metal cations. After a certain period of time (80 and 20 min) almost all the vacant sites got saturated and no further uptake was noticed [29].

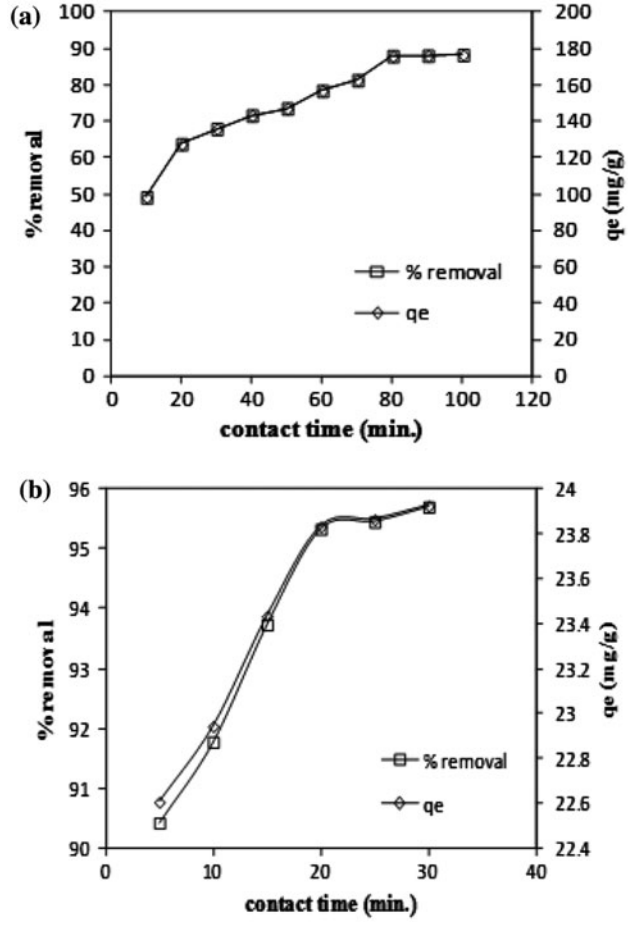

Fig. 5. Effect of contact time on q_e and per cent removal (a) BBR and (b) Cd(II).

Therefore, 80 and 20 min were chosen as the equilibrium contact time for the removal of BBR and Cd(II), respectively.

3.2.2. Effect of adsorbent dose

The removal of BBR and Cd(II) from aqueous solution onto MMWCNT at varying adsorbent doses was studied. With the increase in dose from 0.025 to 0.15 g/L, per cent removal of BBR increased from 82.66 to 89.44 (Fig. 6(a)), whereas the per cent removal of Cd(II) increased from 92.57 to 95.51 with the increase in dose from 0.125 to 1.00 g/L (Fig. 6(b)). Equilibrium was attained at an adsorbent dose of 0.1 and 0.5 g/L for BBR and Cd(II), respectively. The increase in per cent removal with increase in the adsorbent dose could be attributed to the increase in number of vacant sites available to the adsorbate molecules. However, the q_e for both dye and metal was found to decrease with the increase in dose due to an overlap of active sites at high adsorbent doses [30].

3.2.3. Effect of initial concentration of the adsorbate

At an adsorbent dose of 0.1 g/L and a contact time of 80 min, the adsorption capacity of BBR increased from 158.32 to 177.00 mg/g, while per cent removal decreased from 93.04 to 86.14, with an increase in initial concentration from 5 to 25 mg/L, reaching equilibrium at 20 mg/L (Fig. 7(a)). The maximum amount adsorbed under these conditions was 167.07 mg/g (87.84%). For the removal of Cd(II), the q_e increased from 21.54 to 24.11 mg/g, whereas per cent removal decreased from 98.45 to 95.22, with the increase in concentration from 10 to 25 mg/L at an adsorbent dose of 0.5 g/L and 20 min of contact time, reaching equilibrium at 20 mg/L (Fig. 7(b)). The maximum

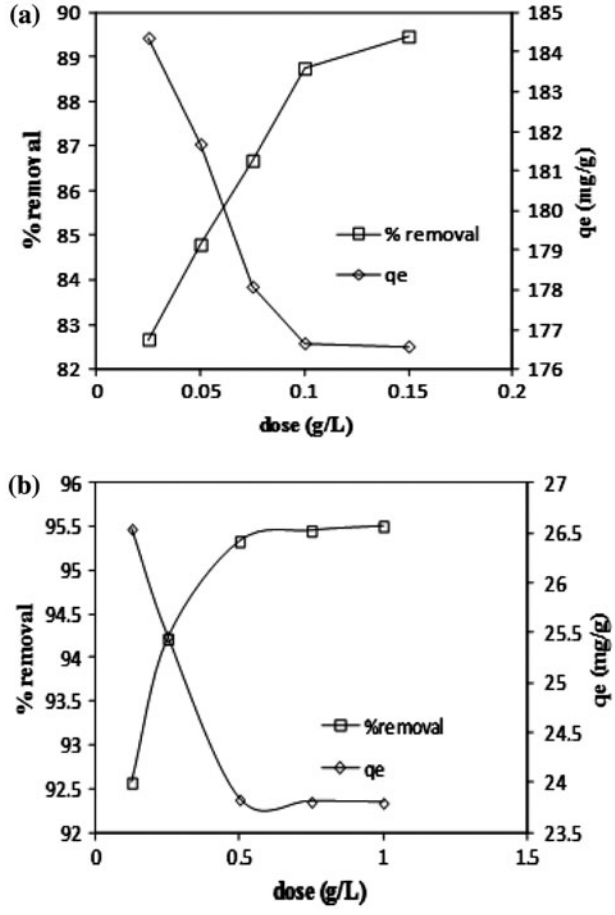

Fig. 6. Effect of dose of MMWCNT on q_e and per cent removal (a) BBR and (b) Cd(II).

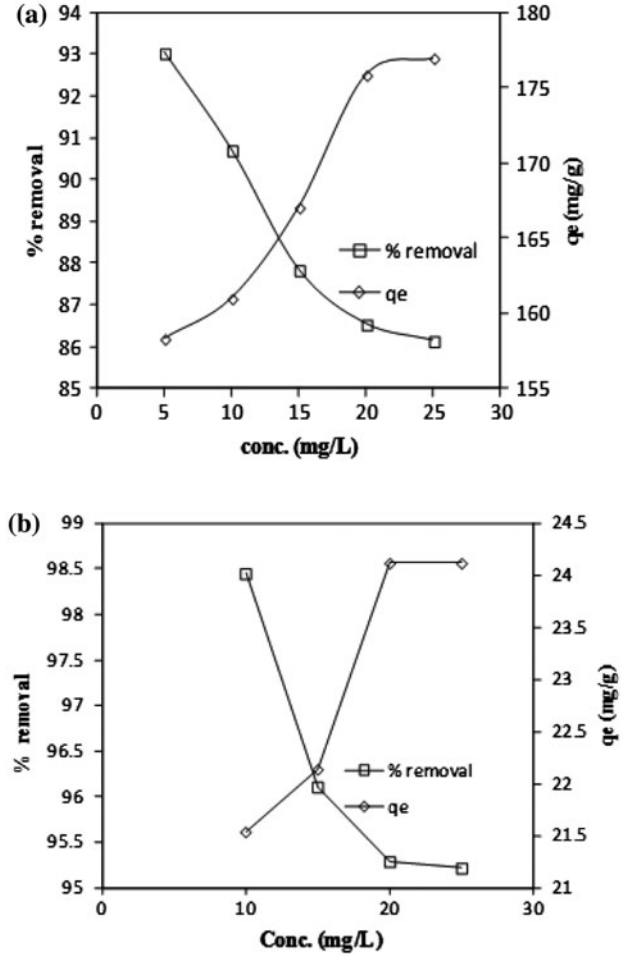

Fig. 7. Effect of initial concentration of (a) BBR and (b) Cd(II) on q_e and per cent removal.

amount of Cd(II) adsorbed under these conditions was 24.12 mg/g (95.29%).

3.2.4. Effect of pH

pH_{pzc} of MMWCNTs was found to be ~4.3 (Fig. 8(a)). At pH < pH_{pzc}, MMWCNT surface is positively charged. As a result, adsorption of positively charged BBR and metal ions decreased due to electrostatic repulsion (Fig. 8(b)). At pH > pH_{pzc}, the surface became negatively charged and hence the adsorption increased due to attractive forces. An equilibrium was established at pH 7 for BBR, while for Cd(II) the adsorption decreased after pH 7 (Fig. 8(c)). For both metal and dye, maximum adsorption was observed at pH 7. Thus, pH 7 was chosen as optimum pH for adsorption studies.

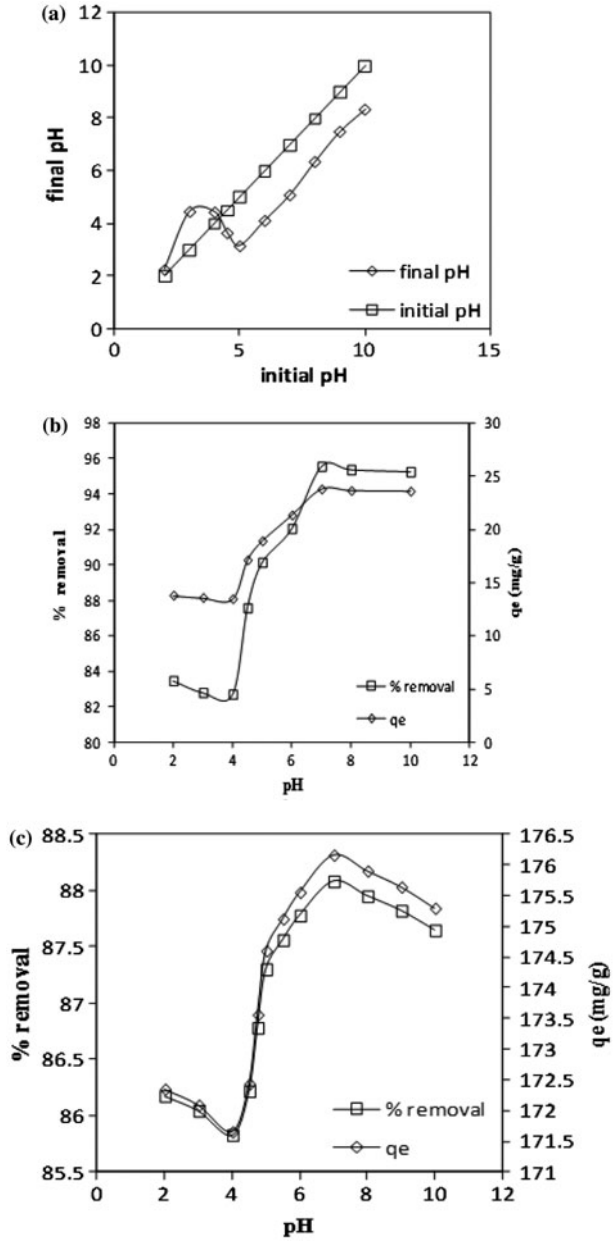

Fig. 8. (a) pHpzc curve of acidified MMWCNT, effect of pH on q_e and per cent removal of (b) BBR and (c) Cd(II).

3.3. Adsorption isotherms

The adsorption data were evaluated using various isotherm models to estimate the nature of adsorption of BBR and Cd(II) onto MMWCNT surface. The isotherm parameters are summarized in Table 2.

3.3.1. Langmuir isotherm model

Langmuir adsorption isotherm is based on the assumption that the adsorbate molecules are adsorbed on definite localized sites with each site being occupied only once, resulting in the formation of a homogenous monolayer.

The linearized Langmuir isotherm can be expressed as [31]:

$$1/q_e = 1/q_m + 1/q_m bC_e \quad (5)$$

where q_m (mg/g) is the amount of dye/metal ions adsorbed per unit weight of adsorbent, b is the equilibrium constant, and were obtained from slope and intercept of Langmuir plots, respectively (Fig. 9(a) and (b)). R^2 values were closer to 1 (Table 2) indicating the applicability of this model for both BBR and Cd(II) ions. This was further supported by R_L values between 0 and 1 (0.74–0.89 for BBR) (0.03–0.48 for Cd(II)) (Table 2) [32].

The adsorption capacity of the MMWCNT as adsorbent was found to be 76.92 mg/g for BBR and 38.17 for Cd(II).

3.3.2. Freundlich isotherm model

The Freundlich adsorption isotherm assumes that the stronger binding sites are occupied first because of which the binding strength goes on decreasing with coverage, resulting in heterogeneous adsorption. The linearized Freundlich isotherm can be expressed as [33]:

$$\log q_e = \log K_f + 1/n_f \log C_e \quad (6)$$

Table 2
Adsorption isotherm parameters for adsorption of BBR and Cd(II)

Isotherm	Isotherm constants	Bismarck brown R			Cd(II)		
		303 K	308 K	313 K	303 K	308 K	313 K
Langmuir	q_m (mg/g)	69.44	71.94	76.92	38.17	29.07	22.99
	b (L/mg)	0.87	0.85	0.79	0.49	1.26	10.87
	R_L	0.74	0.81	0.89	0.48	0.23	0.03
	R^2	0.99	0.99	0.99	0.96	0.99	0.99
Freundlich	n_f	2.48	2.35	2.18	1.64	2.24	5.67
	K_f (L/g)	32.22	32.89	33.69	12.20	15.28	19.53
	R^2	0.99	0.98	0.99	0.94	0.96	0.95
DKR	q_D (mg/g)	52.04	53.44	54.90	24.35	22.43	20.85
	E (kJ/mol)	2.24	2.24	2.24	1.58	2.36	7.07
	R^2	0.93	0.94	0.94	0.99	0.98	0.96
Temkin	K_t (L/g)	7.82	7.25	6.51	3.28×10^{-6}	1.08×10^{-7}	2.25×10^{-9}
	b_t (kJ/mol)	0.16	0.15	0.14	23.26	17.47	7.32
	R^2	0.99	0.99	0.99	0.99	0.99	0.97
Redlich–Peterson	A (L/g)	75.45	72.15	70.42	–	–	–
	B (L/mg)	1.31	1.16	1.06	–	–	–
	g	0.90	0.92	0.92	–	–	–
	R^2	0.99	0.99	0.99	–	–	–

where K_f (L/g) is related to adsorption capacity and n_f is the exponent for favourable adsorption. K_f and n_f were calculated from intercept and slope of Freundlich isotherm, respectively.

On comparing R^2 values (Table 2) for Langmuir and Freundlich isotherms, it was found that the Langmuir isotherm model was better obeyed than Freundlich isotherm model for both dye and metal adsorption. But there was not a significant difference in the R^2 values of the two isotherms in case of BBR adsorption. Therefore, in order to establish whether Langmuir or Freundlich isotherm governs the adsorption of BBR onto MMWCNT, Redlich–Peterson isotherm model was employed.

3.3.3. Redlich–Peterson isotherm model

The Redlich–Peterson isotherm can be described as [34]:

$$q_e = AC_e/1 + BC_e^g \quad (7)$$

where A and B are Redlich–Peterson isotherm constants.

Depending upon the value of g, the equation has two limiting cases.

When the exponent $g = 1$, the Langmuir equation results, given by:

$$q_e = AC_e/1 + BC_e \quad (8)$$

when $g = 0$, Redlich–Peterson isotherm equation transforms to Henry's law given by:

$$q_e = AC_e/1 + B \quad (9)$$

The linear form of Redlich–Peterson equation can be given as follows:

$$\ln[A(C_e/q_e) - 1] = \ln B + g \ln C_e \quad (10)$$

A linear plot between $\ln C_e$ vs. $\ln [A(C_e/q_e) - 1]$ with R^2 values close to 1 (Table 2) suggested the applicability of the model. The equation has three unknowns A, B and g. It was solved by a trial and error procedure using solver function in excel and the values are given in Table 2.

g values close to 1 confirmed that the Langmuir adsorption isotherm is better followed than the Freundlich isotherm model for the adsorption of BBR onto MMWCNT.

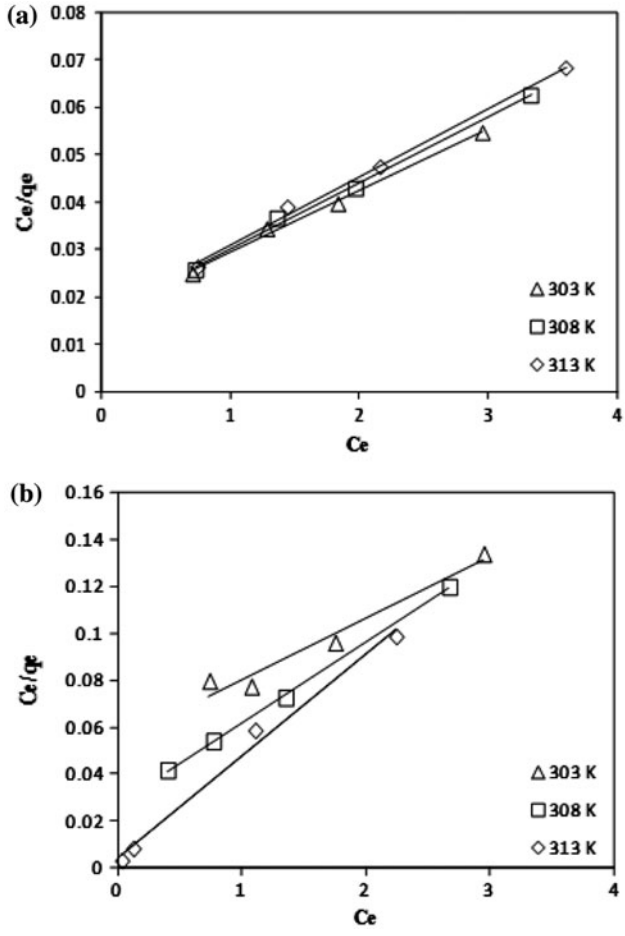

Fig. 9. Langmuir isotherms for adsorption of (a) BBR and (b) Cd(II).

This led to the conclusion that the adsorption of both BBR and Cd(II) onto the adsorbent followed Langmuir isotherm and is, therefore, homogenous and monolayer in nature.

3.3.4. Temkin isotherm model

Temkin noted experimentally that heat of adsorption decreases linearly with coverage but there is a uniform distribution of binding energy. It takes into account indirect adsorbate–adsorbent interactions on adsorbent surface. Temkin adsorption isotherm is expressed as [35]:

$$q_e = RT/b_t \,.\, \ln K_t + RT/b_t \,.\, \ln C_e \quad (11)$$

where R is gas constant, T is temperature in Kelvin, b_t is a constant related to the heat of adsorption and K_t is equilibrium binding constant (L/g) corresponding to maximum binding energy. A linear plot of q_e vs. $\ln C_e$ was obtained at three different temperatures (303, 308 and 313 K) indicating the applicability of Temkin isotherm. The values of b and K_t were determined, respectively, from the slope and intercept of the plot (Table 2). K_t values at 303, 308 and 313 K were 7.82, 7.25 and 6.51 L/g for BBR and 3.28×10^{-6}, 1.08×10^{-7} and 2.25×10^{-9} L/g, for Cd(II), respectively; indicating adsorbate–adsorbent interactions at all temperatures. The values of b_t at these three temperatures were 0.16, 0.15 and 0.14 kJ/mol for BBR and 23.26, 17.47 and 7.32 kJ/mol for Cd(II), indicating an increase in heat of adsorption with increase in coverage as the temperature is decreased.

3.3.5. DKR isotherm model

Dubinin–Kaganer–Radushkevich (DKR) model is useful for calculating the apparent energy of adsorption, which in turn helps to predict whether the adsorption process is physical or chemical in nature. The model can be represented as [36]:

$$\ln q_e = \ln q_D - \beta\varepsilon^2 \quad (12)$$

where $\varepsilon = RT \ln (1 + 1/C_e)$ is Polanyi Potential. The plot of $\ln q_e$ vs. ε^2 yielded straight line, thereby confirming the applicability of the model. The magnitude of β was calculated from the slope of the plot which was used to calculate the magnitude of adsorption energy, E $[=1/(2\beta)^{1/2}]$. The values of E for BBR were found to be equal to 2.24 kJ/mol at all the three temperatures and for Cd(II) values of E were in the range 1.58–7.07 kJ/mol (Table 2). This suggested physical adsorption of both the dye/metal over MMWCNT surface making the recovery process more feasible as there is no actual bond formation between the adsorbate and adsorbent molecules.

Based on the isotherms discussed above, it may be concluded that the adsorption of BBR and Cd(II) was homogenous, monolayer and physical in nature showing considerable adsorbate adsorbent interactions characterized by a non-uniform heat of adsorption but an overall uniform binding energy.

3.4. Column studies

The breakthrough curve (Fig. 10(a) and (b)) indicates that almost all BBR was adsorbed in initial 10 min. Nearly 95% of BBR was adsorbed in 20 min, which was considered breakthrough time (T_b) for its removal. After that the dye concentration in the

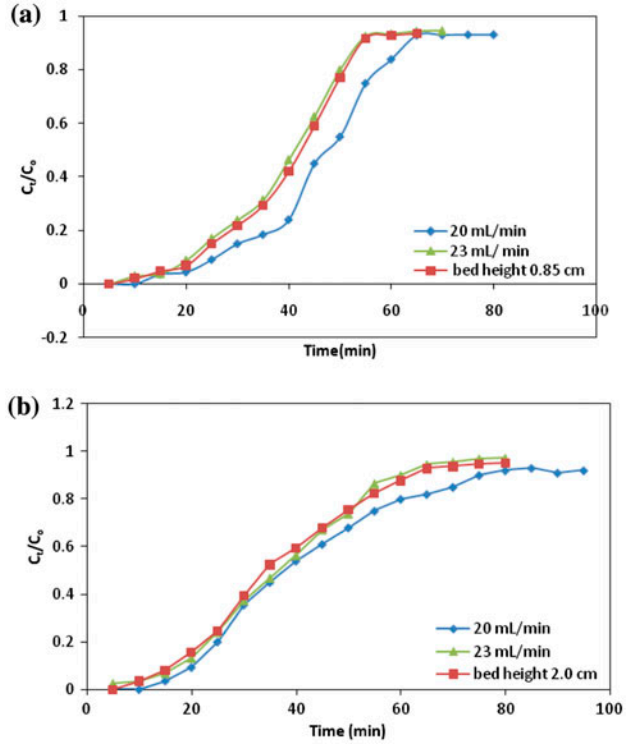

Fig. 10. Breakthrough curve C_e/C_o vs. t (a) BBR and (b) Cd(II).

effluent kept increasing sharply till the column was saturated around 70 min [exhaustion time (T_e)] showing only about 5% adsorption. Similarly, 95% Cd(II) was removed in the initial 15 min (T_b) and saturation occurred at 80 min (T_e). It was concluded that the column showed an efficient removal percentage and that too at a high flow rate (23 mL/min). The column maximum adsorption capacity of 98.16 and 39.15 mg/g, respectively, for BBR and Cd(II) was obtained. The column maximum adsorption capacity q_c (98.16 for BBR; 39.15 mg/g for Cd(II)) was slightly higher than Langmuir (q_m) adsorption capacity (76.92 and 38.17 mg/g for BBR and Cd(II)). The higher value of q_c might be due to the higher adsorbate concentration onto the adsorption zone in comparison to batch process wherein the adsorbate concentration decreases with time gradient.

3.4.1. The Adam–Bohart model

The Adam–Bohart model [37] was applied for the interpretation of the initial part ($C_t/C_o > 0.5$) of the breakthrough curve. The model assumes that the rate of adsorption is proportional to the concentration of the adsorbate species and the remaining capacity of the adsorbent towards targeted adsorbate species [38]. The Adam–Bohart model is given as Eq. (13):

$$\ln(C_o/C_t) = k_{AB}C_o t - k_{AB}N_0(Z/F) \quad (13)$$

where C_o is influent concentration, C_t is the effluent concentration (mg/L) after time, t, k_{AB} is the kinetic constant (L/mg/min), N_0 is the saturation concentration (mg/L) and Z is the bed depth of column (cm), F is the linear flow rate (cm/min). The value of k_{AB} and N_0 were determined from intercept and slope of the linear plot of $\ln(C_t/C_o)$ vs. t. The values of N_0 decreased from 166,703. 6 to 118,264.2 (L/mg/min) for BBR and 71565.3–55466.67 (L/mg/min) for Cd(II) with increasing bed height. When the flow rate was increased from 20 to 23 mL/min N_0 decreased from 166,703. 6 to 145,931.4 (L/mg/min) for BBR and 71,565.3–65,521.7 (L/mg/min) for Cd(II). The results showed that the adsorption kinetics is dominated by external mass transfer in the column adsorption.

3.4.2. The Thomas model

The experimental data were fitted with Thomas model [39], which explains the external and internal diffusion limitation. It is suitable for adsorption obeying the Langmuir isotherm and pseudo-second-order kinetics. Thomas model is expressed as Eq. (14):

$$\ln\{(C_o/C_t) - 1\} = (k_{Th}q_0M/Q) - k_{Th}C_o t \quad (14)$$

where k_{Th} (mL/min/mg) is the Thomas rate constant, q_0 (mg/g) is the Thomas adsorption capacity, M (g) is the mass of adsorbent and Q (mL/min) is the feed flow rate. The values of k_{Th} and q_0 were determined from intercept and slope of the linear plot of $\ln\{(C_t/C_o) - 1\}$ vs. t. The k_{Th} and q_0 values increased with decrease in the bed height from 0.00104 to 0.00085 (mL/min/mg) and 74.86 to 91.03 (mg/g) for BBR and 0.00085 to 0.00099 (mL/min/mg) and 24.09 to 39.14 (mg/g) for Cd(II) at 20 mL/min flow rate. However, with increase in flow rate to 23 mL/min the k_{Th} and q_0 decreased to 0.00105 (mL/min/mg) and 85.72 (mg/g) for BBR and 0.00083 (mL/min/mg) and 32.15 (mg/g) for Cd(II). The R^2 for BBR (0.80–0.97) and Cd(II) (0.93–0.99) is higher than the Adam–Bohart model for BBR (0.83–0.89) and Cd(II) (0.68–0.81) indicating that the Thomas model is better fitted. Moreover, the experimental column adsorption capacity (q_c) is in good accord with Thomas model (q_0).

Table 3
Pseudo-first-order, pseudo-second-order, liquid-film diffusion and intraparticle diffusion rate constants for the adsorption of BBR and Cd(II)

Conc. (mg/L)	Adsorbate		Pseudo-first-order			Pseudo-second-order			Liquid-film diffusion		Intraparticle diffusion	
		$q_{e(exp.)}$ (mg/g)	$q_{e(calc.)}$ (mg/g)	$k_1 \times 10^{-2}$ (1/min)	R^2	$q_{e(calc.)}$ (mg/g)	$k_2 \times 10^{-2}$ (g/mg/min)	R^2	$K_{fd} \times 10^{-2}$ (1/min)	R^2	K_i (mg $min^{0.5}$/g)	R^2
10	Bismarck brown R	25.11	26.42	5.20	0.95	25.77	0.22	0.99	5.21	0.95	1.37	0.99
15		29.22	18.92	4.03	0.95	29.58	0.22	0.99	4.02	0.95	1.33	0.99
20		30.11	14.80	1.38	0.99	31.34	0.21	0.99	1.39	0.99	1.50	0.99
10	Cd(II)	21.54	2.06	10.06	0.99	20.83	18.73	1.00	10.06	0.99	0.43	0.94
15		22.14	1.78	9.90	0.99	22.72	19.07	1.00	9.90	0.99	0.37	0.94
20		24.12	1.66	13.13	0.96	25.00	18.05	0.99	13.12	0.96	0.31	0.97

3.5. Adsorption dynamics

Various kinetic models were studied to predict the mechanism of adsorption and the rate-controlling steps which further led to the idea about order of reaction. The values of different constants of these models are given in Table 3.

3.5.1. Lagergren's pseudo-first-order and pseudo-second-order

The adsorption dynamics was investigated using the Lagergren's pseudo-first-order [40] (Eq. (14)) and pseudo-second-order rate equations [41] (Eq. (15)):

$$\log(q_e - q_t) = \log q_e - k_1 . t/(2.303) \quad (14)$$

$$t/q_t = 1/(k_2 q_e^2) + (1/q_e) . t \quad (15)$$

where q_e and q_t (mg/g) are the amount adsorbed per unit mass at equilibrium and at any time t, k_1 (1/min) and k_2 (g/mg/min) are the pseudo-first-order and pseudo-second-order adsorption rate constants, respectively, and h ($= k_2 q_e^2$) (mg/g min) is the initial adsorption rate at time approaching zero.

k_1 and k_2 values were determined from the slope and intercept of the corresponding plots of $\log(q_e - q_t)$ vs. t, and t/q vs. t (Fig. 11(a) and (b)), respectively, and are tabulated in Table 3 along with correlation coefficients and the $q_{e(calc.)}$ and $q_{e(exp.)}$ values. The calculated q_e values were found to be very close to the experimental q_e values in case of pseudo-second-order rate equation for both BBR and Cd(II). Also the correlation coefficient values for the pseudo-second-order rate equation were found to be very close to 1. In view of these results, it was confirmed that the adsorption of BBR and Cd(II) onto MMWCNT followed pseudo-second-order kinetics.

3.5.2. Intraparticle and liquid film diffusion models

The rate of adsorption at different initial concentrations of the adsorbate was further analysed for

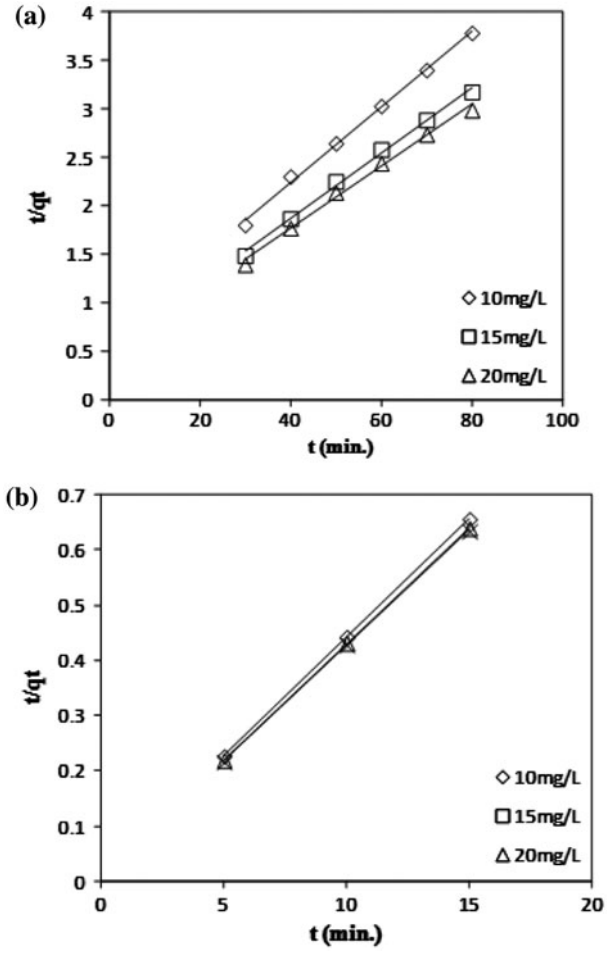

Fig. 11. Pseudo-second-order plots for the adsorption of (a) BBR and (b) Cd(II).

evaluating the role of diffusion in the adsorption process. Adsorption is considered to be a three-step process. The first step involves transport of the adsorbate molecules from the aqueous phase to the film surrounding the adsorbent. In the second step, diffusion of the solute molecules from the film to the adsorbent surface takes place. Finally, in the third step, the adsorbate molecules diffuse into the pore interiors. The first step is bulk diffusion, the second is external mass transfer resistance and the third is intraparticle mass transfer resistance. When the intraparticle mass transfer resistance is the rate-limiting step, then the adsorption process is described as being intraparticle diffusion controlled [42]. The intraparticle diffusion [43] and liquid film diffusion [44] models are given by the following equations:

$$q_t = k_i t^{0.5} + C_i \quad (16)$$

$$-\ln(1-F) = K_{fd} t \quad (17)$$

where k_i (mg/g min$^{0.5}$), K_{fd} (1/min), C_i and F (= q_t/q_e) are rate constants, boundary layer thickness and the fractional attainment of equilibrium at time t, respectively.

The plots of q_t vs. $t^{0.5}$ (Fig. 12(a) and (b)) and ln $(1 - F)$ vs. t (Fig. 13(a) and (b)) for the adsorption system were linear. This indicated that both intraparticle diffusion and liquid film diffusion controlled the adsorption process. However, in either case the plots did not pass through the origin. The deviation of liquid film diffusion plot from the origin may be due to high speed of agitation used during kinetic

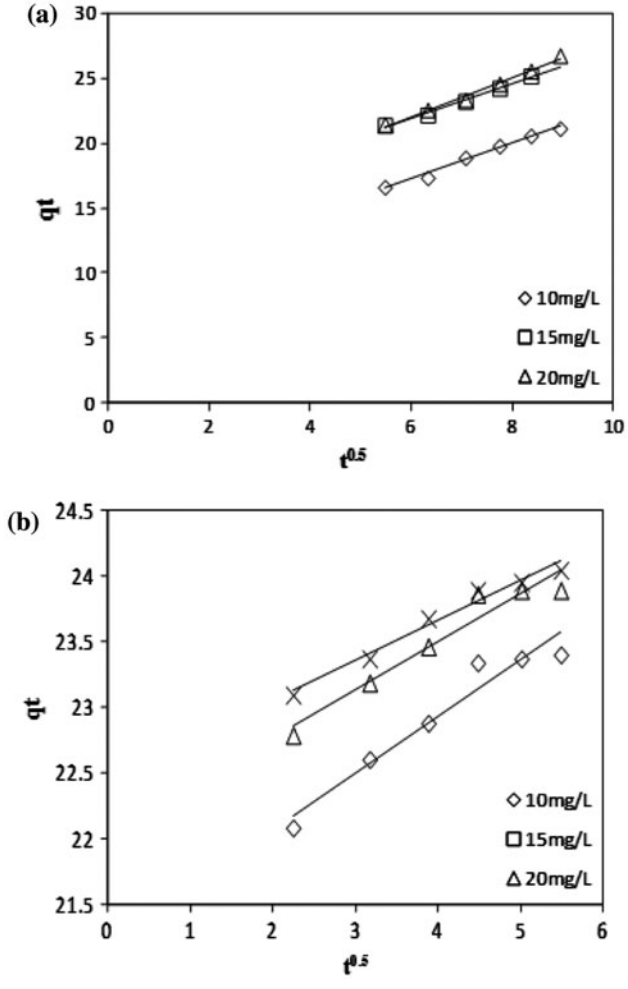

Fig. 12. Intraparticle diffusion plots for the adsorption of (a) BBR and (b) Cd(II).

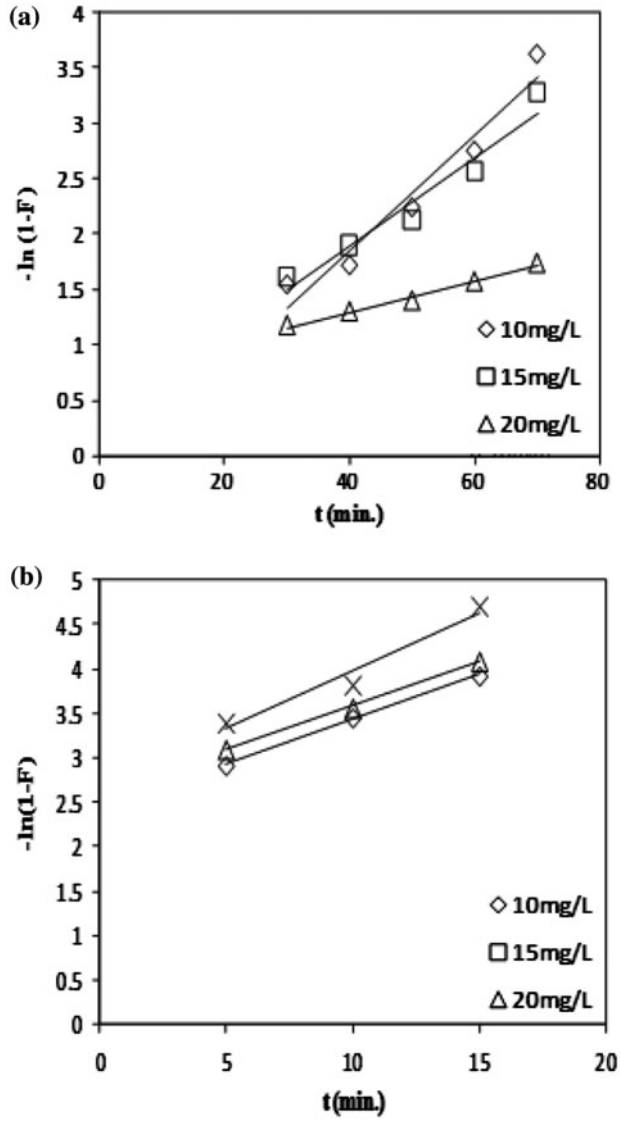

Fig. 13. Liquid film diffusion plots for the adsorption of (a) BBR and (b) Cd(II).

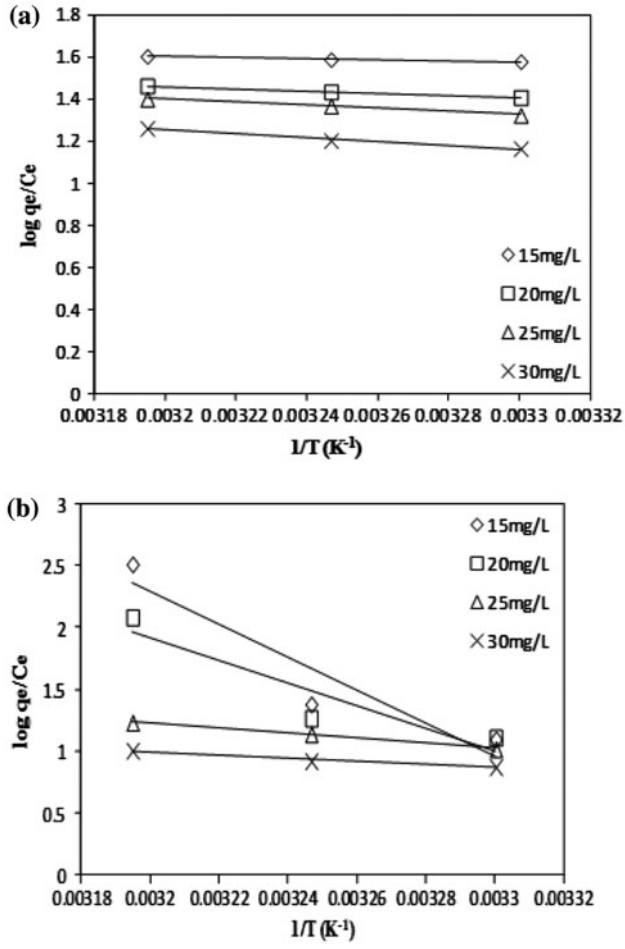

Fig. 14. Thermodynamic plots for the adsorption of (a) BBR and (b) Cd(II).

experiments or may also be due to the difference between rate of mass transfer in the initial and final steps of adsorption [45]. The deviation of intraparticle diffusion plot from the origin indicated that the effect of external film resistance was not negligible. This indicated that both intraparticle diffusion and liquid film diffusion controlled the adsorption process.

3.6. Thermodynamic studies

The thermodynamic parameters for the adsorption system were calculated from van't Hoff's plots of log (q_e/C_e) vs. $1/T$ (Fig. 14(a) and (b)) at different initial concentrations of the dye at different temperatures. The van't Hoff's equation can be expressed as:

$$\log(q_e/C_e) = -\Delta H^\circ/2.303\,RT + \Delta S^\circ/2.303\,R \quad (18)$$

The changes in enthalpy (ΔH°) and entropy (ΔS°) were determined from the slope and intercept, respectively, of van't Hoff's plots. These values are given in Table 4.

The free energy change (ΔG°) was calculated from the following equation:

$$\Delta G^\circ = \Delta H^\circ - T\Delta S^\circ \quad (19)$$

The positive values of ΔH° at different initial concentrations of the dye and metal (Table 4) indicated endothermic nature of the adsorption process. The positive ΔS° values indicated an increased randomness at the solid–solution interface which might be attributed to the displaced water molecules gaining more translational entropy as compared to that lost by the adsorbate molecules during adsorption. Gibbs' free energy change (ΔG°) was negative indicating the adsorption of BBR and Cd(II) on MMWCNT to be spontaneous in nature. Further, ΔG° values became more and more negative on increasing the temperature (Table 4). Hence, a higher temperature was found to be more favourable for this adsorption study.

4. Evaluation of MMWCNT as an adsorbent

A comparison of the adsorption capacity of MMWCNT with other adsorbents in the literature for the removal of BBR and Cd(II) showed that MMWCNT

Table 4
Thermodynamic parameters for adsorption of BBR and Cd(II)

Conc. (mg/L)	Bismarck brown R					Cd(II)				
	ΔH° (kJ/mol)	ΔS° (kJ/mol K)	$-\Delta G^\circ$ (kJ/mol)			ΔH° (kJ/mol)	ΔS° (kJ/mol K)	$-\Delta G^\circ$ (kJ/mol)		
			303 K	308 K	313 K			303 K	308 K	313 K
15	4.53	0.045	9.16	9.38	9.61	255.59	0.86	5.56	9.87	14.18
20	9.91	0.059	8.17	8.47	8.77	175.63	0.60	5.82	8.81	11.81
25	14.07	0.071	7.69	8.05	8.41	390.06	0.15	5.93	6.68	7.42
30	17.50	0.08	6.74	7.14	7.54	240.48	0.01	5.04	5.52	5.99

Table 5
Comparison of adsorption capacities of various adsorbents for removal of BBR and Cd(II)

Adsorbent	Adsorbate	pH, time (h), adsorbent dose (g/L)	Isotherms, kinetics, thermodynamics	Adsorption capacity (mg/g)	Refs.
MMWCNT	Bismarck brown	7 1.33 0.1	Langmuir Pseudo-second-order Spontaneous, endothermic	76.92	This work
Hen feathers	Bismarck brown	3 2 0.2	Langmuir Pseudo-second-order Spontaneous endothermic	302	[1]
Magnetically responsive yeast-based biosorbent	Bismarck brown	– 3 –	Langmuir	75.71	[46]
4-hydroxybenzoic acid-grafted chitosan	Bismarck brown		Langmuir	17.78	[47]
3,4-dihydroxybenzoic acid-grafted chitosan		9		26.18	
3,4-dihydroxyphenylacetic Acid-grafted chitosan		48		39.27	
hydrocaffeic acid-grafted chitosan		–		41.67	
Magnetically modified spent grain	Bismarck brown	– 3 30	Langmuir Freundlich	72.4	[48]
Carbonaceous slurry from fertilizer plant	Bismarck brown		Langmuir	71.5	[49]
Blast furnace sludge		5.5–6.5	First order	8.2	
Blast furnace dust		3	Spontaneous	4.6	
Blast furnace slag		1	exothermic	2.7	
Iron oxide nanospheres	Bismar ck brown		Langmuir	33.80	[50]
HCl-modified iron oxide nanospheres		–	Freundlich Pseudo-second-order	54.90	
α-Ketoglutaricacid-modified magnetic chitosan	Cd(II)	6 0.5 –	Langmuir Pseudo-second-order Spontaneous, endothermic	201.20	[51]
MMWCNT	Cd(II)	7 0.33 0.5	Langmuir Pseudo-second-order Spontaneous, endothermic	38.17	This work
Brewer's spent grain	Cd(II)	5–6 – 0.4	Langmuir, Pseudo-first-order	20.41	[52]
Oxidized multiwalled carbon nanotubes	Cd(II)	5 4 0.5	Langmuir	10.86	[53]
Magnetic oak wood		5	Combined Langmuir-Freundlich (Sips)	2.87	[54]
magnetic oak bark	Cd(II)	48 10	Pseudo-second-order	7.4	
8-hydroxyquinoline-modified multiwalled carbon nanotubes	Cd(II)	7 2 12.5	Langmuir	0.032	[55]
Oxidized multiwalled carbon nanotubes	Cd(II)	5.5 2 1	Langmuir Freundlich Pseudo-second-order	66	[56]
	Cd(II)	5.5 4		2.6 5.1	[57]

(*Continued*)

Table 5 (*Continued*)

Adsorbent	Adsorbate	pH, time (h), adsorbent dose (g/L)	Isotherms, kinetics, thermodynamics	Adsorption capacity (mg/g)	Refs.
H_2O_2 oxidized carbon nanotubes HNO_3oxidized carbon nanotubes $KMnO_4$ oxidized carbon nanotubes		0.5		11.0	
Ferrofluid-modified montmorillonite	Cd(II)	5 24 1	Langmuir Freundlich	63.29	[58]

possessed higher q_m as compared to most other adsorbents and that too at a low contact time and adsorbent dosage at natural pH of most water bodies (7) (Table 5). Additionally, the magnetic nature of the adsorbent facilitates its recovery using a magnetic bar.

5. Conclusions

MMWCNT showed a considerably high BET surface area of 399.67 m^2/g. The optimized conditions for the removal of BBR were 80 min contact time, 0.1 g/L dose of adsorbent, at an initial dye concentration of 20 mg/L at pH 7 and room temperature (298–303 K). For the removal of Cd(II), the optimized conditions were 20 min contact time, 0.5 g/L dose of adsorbent, at an initial dye concentration of 20 mg/L at pH 7 and room temperature (298–303 K). The developed adsorption system was found to be efficient due to higher adsorption efficiency of 76.92 and 38.17 mg/g for BBR and Cd(II), respectively. Langmuir adsorption isotherm gave a better fit than Freundlich for both BBR and Cd(II) suggesting the adsorption process to be homogenous and monolayer in nature. Isotherm studies revealed that both BBR and Cd(II) were adsorbed by physisorption, showing considerable adsorbate adsorbent interactions characterized by a non-uniform heat of adsorption but an overall uniform binding energy. The column studies gave a maximum column capacity of 98.16 and 39.15 mg/g for BBR and Cd(II), respectively, which were comparable to those calculated from batch studies. The experimental data were best described by the Thomas model. Kinetically, the adsorption system followed pseudo-second-order rate kinetics for both dye and metal removal and the process was found to be intraparticle and liquid film diffusion controlled. Thermodynamically, the process was spontaneous and endothermic in nature.

Acknowledgement

One of the authors, Momina Nazir, is thankful to the University Grants Commission (UGC), New Delhi, India for financial assistance (BSR fellowship).

References

[1] J. Mittal, V. Thakur, A. Mittal, Batch removal of hazardous azo dye Bismark Brown R using waste material hen feather, Ecol. Eng. 60 (2013) 249–253.
[2] G.M. Sole, J.K. Chipman, The mutagenic potency of chrysoidines and Bismark brown dyes, Carcinogenesis 7 (1986) 1921–1923.
[3] V.K. Gupta, Suhas, Application of low-cost adsorbents for dye removal—A review, J. Environ. Manage. 90 (2009) 2313–2342.
[4] T.A. Khan, V. Singh, I. Ali, Sorption of Cd(II), Pb(II), and Cr(VI) metal ions from wastewater using bottom fly ash as a low cost sorbent, J. Environ. Protect. Sci. 3 (2009) 124–132.
[5] T.A. Khan, S. Dahiya, I. Ali, Removal of direct red 81 dye from aqueous solution by native and citric acid modified bamboo sawdust—Kinetic study and equilibrium isotherm analyses, Gazi Univ. J. Sci. 25 (2012) 59–87.
[6] T.A. Khan, M. Nazir, Enhanced adsorptive removal of a model acid dye bromothymol blue from aqueous solution using magnetic chitosan-bamboo sawdust composite: Batch and column studies, Environ. Prog. Sustainable Energy 34 (2015) 1444–1454.
[7] T.A. Khan, M. Nazir, E.A. Khan, Adsorptive removal of rhodamine B from textile wastewater using water chestnut (*Trapa natans* L.) peel: Adsorption dynamics and kinetic studies, Toxicol. Environ. Chem. 95 (2013) 919–931.
[8] K. Zare, V.K. Gupta, O. Moradi, A.S.H. Makhlouf, M. Silanpaa, M.N. Nadagouda, H. Sadegh, R. Shahryari-ghoshekandi, A. Pal, Z. Wang, I. Tyagi, M. Kazemi, A comparative study on the basis of adsorption capacity between CNTs and activated carbon as adsorbents for removal of noxious synthetic dyes: A review, J. Nanostruct. Chem. 5 (2015) 227–236.
[9] J. Liang, J. Liu, X. Yuan, H. Dong, G. Zeng, H. Wu, H. Wang, J. Liu, S. Hua, S. Zhang, Z. Yu, X. He, Y. He, Facile synthesis of alumina-decorated multi-walled carbon nanotubes for simultaneous adsorption of cadmium ion and trichloroethylene, Chem. Eng. J. 273 (2015) 101–110.
[10] M.I. Mohammed, A.A.A. Razak, D.A.H. Al-Timimi, Modified multiwalled carbon nanotubes for treatment of some organic dyes in wastewater, Adv. Mater. Sci. Eng. (2014), doi: 10.1155/2014/201052.
[11] N.A. Kabbashi, M.A. Atieh, A. Al-Mamun, M.E.S. Mirghami, M.Z. Alam, N. Yahya, Kinetic adsorption of application of carbon nanotubes for Pb(II) removal from aqueous solution, J. Environ. Sci. 21 (2009) 539–544.

[12] F.M. Machado, C.P. Bergmann, E.C. Lima, B. Royer, F.E. de Souza, I.M. Jauris, T. Calvete, S.B. Fagan, Adsorption of Reactive Blue 4 dye from water solutions by carbon nanotubes: Experiment and theory, Phys. Chem. Chem. Phys. 14 (2012) 11139–11153.
[13] L. Ji, L. Zhou, X. Bai, Y. Shao, G. Zhao, Y. Qu, C. Wang, Y. Li, Facile synthesis of multiwall carbon nanotubes/iron oxides for removal of tetrabromobisphenol A and Pb(II), J. Mater. Chem. 22 (2012) 15853–15862.
[14] L. Xu, J. Li, M. Zhang, Adsorption characteristics of a novel carbon-nanotube-based composite adsorbent towards organic pollutants, Ind. Eng. Chem. Res. 54 (2015) 2379–2384.
[15] X. Ren, C. Chen, M. Nagatsu, X. Wang, Carbon nanotubes as adsorbents in environmental pollution management: A review, Chem. Eng. J. 170 (2011) 395–410.
[16] R. Sivashankar, A.B. Sathya, K. Vasantharaj, V. Sivasubramanian, Magnetic composite an environmental super adsorbent for dye sequestration—A review, Environ. Nanotechnol. Monit. Manage. 1–2 (2014) 36–49.
[17] W.W. Tang, G.M. Zeng, J.L. Gong, Y. Liu, X.Y. Wang, Y.Y. Liu, Z.F. Liu, L. Chen, X.R. Zhang, D.Z. Tu, Simultaneous adsorption of atrazine and Cu(II) from wastewater by magnetic multi-walled carbon nanotube, Chem. Eng. J. 211–212 (2012) 470–478.
[18] J.-L. Gong, B. Wang, G.-M. Zeng, C.-P. Yang, C.-G. Niu, Q.-Y. Niu, W.-J. Zhou, Y. Liang, Removal of cationic dyes from aqueous solution using magnetic multi-wall carbon nanotube nanocomposite as adsorbent, J. Hazard. Mater. 164 (2009) 1517–1522.
[19] H. Gao, S. Zhao, X. Cheng, X. Wang, L. Zheng, Removal of anionic azo dyes from aqueous solution using magnetic polymer multi-wall carbon nanotube nanocomposite as adsorbent, Chem. Eng. J. 223 (2013) 84–90.
[20] T. Madrakian, A. Afkhami, M. Ahmadi, H. Bagheri, Removal of some cationic dyes from aqueous solutions using magnetic-modified multi-walled carbon nanotubes, J. Hazard. Mater. 196 (2011) 109–114.
[21] F.H. Malayeri, M.R. Sohrabi, H. Ghourchian, Magnetic multi-walled carbon nanotube as an adsorbent for toluidine blue o removal from aqueous solution, Int. J. Nanosci. Nanotechnol. 8 (2012) 79–86.
[22] H. Huang, J. Yu, X. Jiang, Preparation of magnetic oxidized multi-walled carbon nanotubes for the adsorption of rhodamine B in aqueous solution, Nano 09 (2014) 1450093, doi: 10.1142/S1793292014500933.
[23] H. Wang, A. Zhou, F. Peng, H. Yu, J. Yang, Mechanism study on adsorption of acidified multiwalled carbon nanotubes to Pb(II), J. Colloid Interface Sci. 316 (2007) 277–283.
[24] P. Berger, N.B. Adelman, K.J. Beckman, D.J. Campbell, A.B. Ellis, G.C. Lisensky, Preparation and properties of an aqueous ferrofluid, J. Chem. Educ. 76 (1999) 943–948.
[25] T.A. Khan, S.A. Chaudhry, I. Ali, Equilibrium uptake, isotherm and kinetic studies of Cd(II) adsorption on to iron oxide activated red mud from aqueous solution, J. Mol. Liq. 202 (2015) 165–175.
[26] C. Chen, X. Wang, Adsorption of Ni(II) from aqueous solution using oxidized multi-wall carbon nanotubes, Ind. Eng. Chem. Res. 45 (2006) 9144–9149.
[27] J. Hu, I.M.C. Lo, G. Chen, Performance and mechanism of chromate(VI) adsorption by δ-FeOOH-coated maghemite (γ-Fe_2O_3) nanoparticles, Sep. Purif. Technol. 58 (2007) 76–82.
[28] X. Peng, Z. Luan, Z. Di, Z. Zhang, C. Zhu, Carbon nanotubes-iron oxides magnetic composites as adsorbent for removal of Pb(II) and Cu(II) from water, Carbon 43 (2005) 855–894.
[29] Y.F. Shen, J. Tang, Z.H. Nie, Y.D. Wang, Y. Ren, L. Zuo, Preparation and application of magnetic Fe_3O_4 nanoparticles for wastewater purification, Sep. Purif. Technol. 68 (2009) 312–319.
[30] V.K. Garg, R. Gupta, A.B. Yadav, R. Kumar, Dye removal from aqueous solution by adsorption on treated sawdust, Bioresour. Technol. 89 (2003) 121–124.
[31] I. Langmuir, The adsorption of gases on plane surfaces of glass, mica and platinum, J. Am. Chem. Soc. 40 (1918) 1361–1403.
[32] K.R. Hall, L.C. Eagleton, A. Acrivos, T. Vermeulen, Pore- and solid-diffusion kinetics in fixed-bed adsorption under constant-pattern conditions, Ind. Eng. Chem. Fundam. 5 (1966) 212–223.
[33] H.Z. Freundlich, Over the adsorption in solution, J. Phys. Chem. 57A (1906) 385–470.
[34] O. Redlich, D.L. Peterson, A useful adsorption isotherm, J. Phys. Chem. 63 (1959) 1024.
[35] M.I. Temkin, V. Pyzhev, Kinetic of ammonia synthesis on promoted iron catalyst, Acta Physiochim USSR 12 (1940) 327–356.
[36] M.M. Dubinin, L.V. Radushkevich, The equation of the characteristic curve of activated charcoal, Dokl. Akad. Nauk. USSR 55 (1947) 327–329.
[37] G.S. Bohart, E.Q. Adams, Some aspects of the behavior of charcoal with respect to chlorine. 1, J. Am. Chem. Soc. 42 (1920) 523–544.
[38] A. Maiti, S. DasGupta, J.K. Basu, S. De, Batch and column studies: Adsorption of arsenate using untreated laterite as adsorbent, Ind. Eng. Chem. Res. 47 (2008) 1620–1629.
[39] H.C. Thomas, Heterogeneous ion exchange in a flowing system, J. Am. Chem. Soc. 66 (1944) 1466–1664.
[40] S. Lagergren, About the theory of so-called adsorption of soluble substances, K. Svenska Vet. Acad. Handlingar 24 (1898) 1–39.
[41] Y.S. Ho, G. McKay, Pseudo-second order model for sorption processes, Process Biochem. 34 (1999) 451–465.
[42] J.C. Igwe, A.A. Abia, Adsorption kinetics and intraparticulate diffusivities for bioremediation of Co(II), Fe(II) and Cu(II) ions from waste water using modified and unmodified maize cob, Int. J. Phys. Sci. 2 (2007) 119–127.
[43] W.J. Weber, J.C. Morris, Advances in Water Pollution Research, Pergamon Press, Oxford, 1964.
[44] G.E. Boyd, A.M. Adamson, L.S. Myers, The exchange adsorption of ions from aqueous solution bioorganic zeolites II, Kinetics, J. Am. Chem. Soc. 69 (1949) 2836–2842.
[45] E.-S.Z. El-Ashtoukhy, N.K. Amin, O. Abdelwahab, Removal of lead(II) and copper(II) from aqueous solution using pomegranate peel as a new adsorbent, Desalination 223 (2008) 162–173.
[46] I. Safarik, L.F.T. Rego, M. Borovska, E. Mosiniewicz-Szablewska, F. Weyda, M. Safarikova, New magnetically

responsive yeast-based biosorbent for the efficient removal of water-soluble dyes, Enzyme Microb. Technol. 40 (2007) 1551–1556.
[47] A.-C. Chao, S.-S. Shyu, Y.-C. Lin, F.-L. Mi, Enzymatic grafting of carboxyl groups on to chitosan—To confer on chitosan the property of a cationic dye adsorbent, Bioresour. Technol. 91 (2004) 157–162.
[48] I. Safarik, K. Horska, M. Safarikova, Magnetically modified spent grain for dye removal, J. Cereal Sci. 53 (2011) 78–80.
[49] A. Bhatnagar, A.K. Jain, A comparative adsorption study with different industrial wastes as adsorbents for the removal of cationic dyes from water, J. Colloid Interface Sci. 281 (2005) 49–55.
[50] M. Khosravi, B. Yahyaei, S. Azizian, Adsorption of bismarck brown by iron oxide nanosphere and its modified form, J. Dispersion Sci. Technol. 35 (2014) 1135–1142.
[51] G. Yang, L. Tang, X. Lei, G. Zeng, Y. Cai, X. Wei, Y. Zhou, S. Li, Y. Fang, Y. Zhang, Cd(II) removal from aqueous solution by adsorption on α-ketoglutaric acid-modified magnetic chitosan, Appl. Surf. Sci. 292 (2014) 710–716.
[52] R.O.A. Adelagun, A.U. Itodo, E.P. Berezi, O.J. Oko, E.A. Kamba, C. Andrew, H.A. Bello, Adsorptive removal of Cd^{2+} and Zn^{2+} from aqueous system by BSG, Chem. Mater. Res. 6 (2014) 104–112.
[53] Y.-H. Li, J. Ding, Z. Luan, Z. Di, Y. Zhu, C. Xu, D. Wu, B. Wei, Competitive adsorption of Pb, Cu and Cd ions from aqueous solutions by multiwalled carbon nanotubes, Carbon 41 (2003) 2787–2792.
[54] D. Mohan, H. Kumar, A. Sarswat, M. Alexandre-Franco, C.U. Pittman Jr, Cadmium and lead remediation using magnetic oak wood and oak bark fast pyrolysis bio-chars, Chem. Eng. J. 236 (2014) 513–528.
[55] S.A. Kosa, G. Al-Zhrani, M.A. Salam, Removal of heavy metals from aqueous solutions by multi-walled carbon nanotubes modified with 8- hydroxyquinoline, Chem. Eng. J. 181–182 (2012) 159–168.
[56] M.R. Lasheen, I.Y. El-Sherif, D.Y. Sabry, S.T. El-Wakeel, M.F. El-Shahat, Removal of heavy metals from aqueous solution by multiwalled carbon nanotubes: Equilibrium, isotherms, and kinetics, Desalin. Water Treat. 51 (2013) 1–10.
[57] Y.-H. Li, S. Wang, Z. Luan, J. Ding, C. Xu, D. Wu, Adsorption of cadmium(II) from aqueous solution by surface oxidized carbon nanotubes, Carbon 41 (2003) 1057–1062.
[58] A. Mockovčiaková, Z. Orolínová, J. Škvarla, Enhancement of the bentonite sorption properties, J. Hazard. Mater. 180 (2010) 274–281.